Research Article

Marwa Nabil, Mohamed Elnouby*, Abdulaziz A. Al-Askar, Przemysław Łukasz Kowalczewski, Ahmed Abdelkhalek*, Said I. Behiry

Porous silicon nanostructures: Synthesis, characterization, and their antifungal activity

https://doi.org/10.1515/chem-2023-0169
received July 5, 2023; accepted November 20, 2023

Abstract: The use of synthetic pesticides has come under scrutiny, and there has been a subsequent shift toward the investigation of alternative methods for the treatment of plant diseases. One notable advancement in this field is the utilization of porous silicon (PS) powder as a sustainable antifungal agent. The synthesis of PS nanoparticle (PS-NP) powder was carried out using the environmentally friendly ultrasonication process. X-ray powder diffraction, Fourier transform infrared spectroscopy, Raman spectroscopy, UV-VIS absorbance, and photoluminescence were some of the methods used to characterize PS-NPs. The different characterization methods revealed the formation of a nanocrystalline structure possessing a cubic Si crystalline quality. The crystal size of PS-NPs, as determined from X-ray diffractometer data, ranges from 36.67 to 52.33 nm. The obtained PS has a high band gap of 3.85 eV and presents a photoluminescence peak at 703 nm. The antifungal activity of the synthesized PS-NPs was assessed against three molecularly characterized fungi, namely *Rhizoctonia solani*, *Fusarium oxysporum*, and *Botrytis cinerea*, which were obtained from tomato plants. The concentration of PS-NPs at 75 µg/mL exhibited the highest enhancement in growth inhibition percentages as compared to the control group. *R. solani* had the highest inhibition percentage of 82.96%. In conclusion, the encouraging structural properties and antimicrobial capabilities of PS-NPs pave the way for their application across diverse technological industries. To the best of our knowledge, this is the first *in vitro* study of PS-NPs to evaluate their fungal control efficiency.

Keywords: porous silicon, antifungal activity, ITS, synthesis, XRD, Raman, FTIR, UV-VIS, ultrasonication

1 Introduction

Nanomaterials have attracted scientists' interest owing to their unique physical, chemical, and biological properties. They can be used for many purposes, like controlling plant pathogens, which makes them an unusual way to get rid of pests [1–3]. Silicon (Si) element is a significant element that is essential for several physiological and metabolic processes in plants [4]. Si is widely regarded as the predominant semiconductor material due to its versatile applications in various electrical devices such as transistors, solar cells, integrated circuits, and others [5]. These may be due to its significant band gap, expansive optical transmission range, extensive absorption spectrum, surface roughening, and effective anti-reflection coating.

Porous silicon (PS) is widely recognized as a fundamental component in numerous contemporary industries across various domains, including metallurgy, electronics, and photonics. This technology has the potential to be applied in various domains, including microelectronics, optoelectronics, chemical, and biological sensors, as well as biomedical devices [6]. PS can be prepared using a large number of techniques, including anodic etching [7,8], spark plasma sintering stain etching, hydrothermal erosion, and stain chemical etching (i.e., acidic and alkaline) [9,10]. PS

*** Corresponding author: Mohamed Elnouby,** Advanced Technology and New Materials Research Institute, City for Scientific Research and Technology Applications, New Borg El-Arab City, Alexandria, 21934, Egypt, e-mail: m_nano2050@yahoo.com, tel: +201007556883
*** Corresponding author: Ahmed Abdelkhalek,** Plant Protection and Biomolecular Diagnosis Department, Arid Lands Cultivation Research Institute, City of Scientific Research and Technological Applications, Alexandria 21934, Egypt, e-mail: aabdelkhalek@srtacity.sci.eg, tel: +201007556883
Marwa Nabil: Electronic Materials Researches Department, Advanced Technology and New Materials Research Institute, City for Scientific Research and Technology Applications, New Borg El-Arab City, Alexandria, 21934, Egypt, e-mail: marwamoh2000@yahoo.com
Abdulaziz A. Al-Askar: Department of Botany and Microbiology, College of Science, King Saud University, P.O. Box 2455, Riyadh 11451, Saudi Arabia, e-mail: aalaskara@ksu.edu.sa
Przemysław Łukasz Kowalczewski: Department of Food Technology of Plant Origin, Poznań University of Life Sciences, Poznań, Poland, e-mail: przemyslaw.kowalczewski@up.poznan.pl
Said I. Behiry: Agricultural Botany Department, Faculty of Agriculture (Saba Basha), Alexandria University, Alexandria 21531, Egypt, e-mail: said.behiry@alexu.edu.eg

Open Access. © 2024 the author(s), published by De Gruyter. This work is licensed under the Creative Commons Attribution 4.0 International License.

nanoparticles (PS-NPs) exhibit considerable potential in various fields such as sensor technology, theragnostic applications, antibacterial interventions, antiviral therapy, among others. The composition of PS-NPs comprises elementary silicon and its potential compounds, including surface oxides. It exhibits the notable attribute of having low cytotoxicity. One notable characteristic of PS-NPs is their ability to undergo biodegradation, resulting in the formation of non-toxic silicic acid [11]. The antimicrobial activity was enhanced by the metal and metal oxide nanoparticles, whether used individually or in nanocomposite structures, due to their increased range of improved characteristics [12]. PS-NPs were synthesized using an ultrasonication technique and an alkali wet chemical etching process (in a single step) with commercially available silicon powder. This method holds great promise due to its safety, cost-effectiveness, and high yield percentage [9].

The utilization of Si nanoparticles (Si-NPs) was observed to mitigate the oxidative stress response through the activation of defense mechanisms in the presence of biotic and abiotic stressors [13,14]. Si-NPs are promising for making effective fertilizers for crops. This is due to their ability to minimize fertilizer loss through a gradual and regulated release mechanism, thereby facilitating timely and responsive delivery [15]. The application of Si-NPs was observed to enhance the germination of seeds in *Cucurbita pepo* [16] and the photosynthetic rate of tomato plants [17]. Silicon might be a part of the system by which plants and pathogens interact, trigger the host's defense reaction, and cause plants to make a series of small-molecule metabolites that make them more resistant to disease [18,19]. Si-NPs boost the amount of phenolics in *F. oxysporum*-infected corn, which helps the corn resist phytopathogens [18]. It has been observed that silicon modulates the activities of plant resistance enzymes [20–22]. El-Shetehy et al. [23] have recently documented that Si-NPs trigger systemic acquired resistance, resulting in a reduced incidence of *Pseudomonas syringae*-induced diseases in *Arabidopsis thaliana* [23]. The utilization of PS-NPs as antibacterial and antifungal agents is a relatively recent concept, as there has been a shift in focus towards the development of non-toxic and safe nanoparticles. It has been shown in many studies that nanoparticles like silver and selenium can be used to control *R. solani, F. oxysporum*, and *B. cinerea*. The potential impact of PS-NPs against these pathogens aligns with the findings of the aforementioned studies.

Fungal-induced plant diseases currently pose a significant threat to global agriculture, potentially jeopardizing the food security of certain nations and leading to substantial economic losses estimated in the billions [24,25]. The tomato plant is a very valuable crop that possesses diverse properties, making it a commonly utilized source of sustenance for human consumption. It serves as a staple food in both affluent and economically disadvantaged nations. Increasing the cultivation of this particular crop is a prominent agricultural objective in several nations, such as Egypt, Sudan, Algeria, and other relevant countries, mostly driven by the consistent growth in demand. Hence, the primary aims of this investigation were as follows: (a) to produce PS-NPs through the process of ultrasonication; (b) to conduct a comprehensive characterization of PS-NPs using techniques such as X-ray powder diffraction, Fourier transform infrared (FTIR) spectroscopy, Raman spectroscopy, UV-VIS absorbance, and photoluminescence; (c) to identify the specific fungal pathogens responsible for the occurrence of dry rot and gray mold in tomato plants; (d) to perform both morphological and molecular characterization of the isolated fungi; and (e) to evaluate the antifungal properties of PS-NPs against the fungi *R. solani*, *F. oxysporum*, and *B. cinerea*. To the best of our knowledge, this study represents the initial *in vitro* investigation of PS-NPs in order to assess their effectiveness in controlling fungal growth.

2 Materials and methods

This section outlines the methodology for the preparation of PS powder and presents relevant assays to characterize the material, thereby demonstrating its potential application as an antifungal agent. The subsequent section also encompassed a biological investigation aimed at monitoring the impact and efficacy of utilizing PS powder.

2.1 PS-NP powder preparation and characterization

Commercially available silicon powder (Si-powder) (Silicium, Pulver, 99%) was used. The synthesis of PS-NP powder was carried out using the anisotropic alkali chemical etching process via ultrasonication (Ultra-Sonic 208H, KSU-600) [26]. The alkaline, high-oxidant mixture contained 3 wt% KOH and 30 vol% *n*-propanol. It was exposed to ultrasonication waves for 3 h. The powder product was filtered, washed, and then dried overnight at 40°C to obtain the PS-NP powder. X-ray diffractometer (XRD) was employed to characterize the powder structure, crystallographic phase, and crystal size of PS-NP samples. XRD analysis was conducted using Cu-Kα radiation with a wavelength of 1.5405 Å and at a scanning rate of 4° per min on a 7000 Schimadzu diffractometer located in the United States. The chemical bond formation

was determined using a Fourier transform infrared (FTIR) spectrophotometer (Shimadzu FTIR-8400s, Japan). FTIR spectroscopy was also employed to investigate multiple vibration modes, with each infrared spectrum being recorded in the range of 400–4,000 cm^{-1}. Raman spectroscopy was conducted using the Senteral-Bruker Raman micro-spectroscopy instrument. UV-Vis spectroscopy was performed using the Spectrophotometer Double Auto Cell from Labomed Inc., USA. Additionally, photoluminescence measurements were carried out using the Cary Eclipse Fluorescence Spectrophotometer Photoluminescence Instrument from America.

2.2 Fungal study

2.2.1 Isolation

In this study, a systematic procedure was followed to isolate the fungi from tomato roots and fruits exhibiting symptoms such as rot, wilting, or visible fungal growth. Initially, the tomato samples were meticulously cleaned with water to eliminate any visible dirt or debris present on the surfaces. Subsequently, tomatoes were subjected to a sterilization step by immersing in a 70% ethanol (Merck KGaA, Darmstadt, Germany) solution for 1 min. This ethanol treatment effectively sterilized the external surfaces of the tomatoes. To ensure the removal of any residual ethanol, tomatoes were thoroughly rinsed with sterile distilled water, thus completing the surface sterilization process. Small pieces (1–2 cm^2) were cut from the tomato parts using a sterile scalpel. The tomato tissue samples were placed on the surface of sterile potato dextrose agar (PDA) (Merck KGaA, Darmstadt, Germany) Petri dishes. The Petri dishes were sealed with parafilm and incubated at a temperature of 25 ± 2°C in an incubator ICB-125B (Bioevopeak Co., Ltd., Jinan, Shandong, China). After 7 days of incubation, the Petri dishes were observed for fungal growth. Once distinct fungal colonies appeared they were carefully transferred to new PDA-Petri dishes using a sterile scalpel. Each isolated colony was ensured to originate from a single fungal spore or mycelium to maintain pure cultures. The Petri dishes were labeled with the isolate's coded names, dates, and any other relevant information. The isolates were kept in the refrigerator at 4°C until further examination.

2.2.2 Identification of the tested fungi

Fungi were identified morphologically by their macroscopic and microscopic traits. Infected tissues were evaluated for the presence of brown, sunken lesions with a distinctive collar-like margin. Wilting, yellowing, and vascular discoloration were examined. Brown or reddish-brown lesions may be present on the lower stem. Grayish-brown fuzzy fungal growth on the surface of infected tissues and grayish spore masses were looked for under high humidity conditions.

For microscopic examination, a small piece of infected tissue was placed on a clean glass slide, and a drop of lactophenol cotton blue solution was added. It was then covered with a coverslip. Under a VWR 384 BL384 P microscope (Labotec company, Cape Town, South Africa) at low magnification (40×) and high magnification (100×), the hyphal growth and conidia were observed and characterized.

For molecular studies, we initially started with fungal DNA extraction, which was extracted from the pure cultures using a cetyltrimethylammonium bromide extraction method [27].

The PCR (Techne Prime Thermal Cycler, Cole Parmer, IL, USA) amplification of the internal transcribed spacer (ITS) region was performed with specific primers, ITS1 and ITS4 [28]. The success of PCR amplification was verified by running the PCR products on a 1% agarose gel electrophoresis (Thermo Fisher Scientific Inc., Waltham, MA, USA). The PCR products were purified to remove excess primers and nucleotides. The purified PCR products were submitted to a DNA sequencing service using a DNA sequencer (ABI 3730xl System, Thermo Fisher Scientific Inc., Waltham, MA, USA). The raw DNA sequencing data for each sample were obtained and deposited in the GenBank portal under accession numbers.

2.2.3 PS-NP antifungal activity

The food poisoning technique was used to assess the antifungal activity of PS-NPs against isolated fungi [29,30]. The PS-NPs were sterilized by autoclaving (VASI-50L Vertical Autoclave, KEWLAB Pty Ltd, Melbourne, Australia). A suspension of the nanoparticles was prepared by dispersing them in sterile distilled water. The PS-NP concentrations were adjusted by weight per volume (w/v) in the PDA medium to 25, 50, 75, and 100 µg/mL before being poured into Petri dishes and allowed to solidify.

A mycelial plug of each fungal isolate was transferred to the center of individual food poisoning plates using a sterile scalpel. Negative control plates were prepared by applying sterile distilled water without the nanoparticles. The positive control plates were prepared by dissolving 10 µg/mL of sterile distilled water in PDA to assess fungal growth in the absence of nanoparticles.

The Petri dishes were sealed with parafilm and incubated at 25 ± 2°C for fungal growth. After the incubation period, the plates were observed for the growth of fungal colonies. The diameter of the fungal growth inhibition was measured and compared with the control plates [31].

2.3 Data analysis

The observations were recorded, and the inhibition percentage % was measured for each fungal isolate. A statistical analysis, such as an analysis of variance, was performed to determine the significance of the antifungal activity of the PS-NPs.

3 Results and discussion

3.1 XRD analysis

Figure 1 shows the XRD pattern of the prepared PS powder. It was observed that all peaks were indexed to the cubic Si phase with a space group *Fd*-3*m* (227) and lattice parameters $a = b = c = 5.4309$ Å (ICDD Card No. 00-027-1402). In addition, the low-intensity broad band around $2\Theta = 25°$ may be attributed to the amorphous silicon part. The full width at half-maximum (FWHM) of the peaks are observed around 28.26°, 47.16°, 55.96°, 69°, and 76.28°, which correspond to (111) [32], (220) [33], (311) [34], (400) [35], and (331) [9], respectively (Table 1). These findings are in good agreement with those of other researchers. Fakhri et al. [36] reported that GaN-NPs are crystalline with a mixture of cubic and hexagonal phases and were prepared by the laser ablation method.

The crystal sizes of the obtained nanoparticles were calculated using the Debye–Scherer equation [37]

$$D = \frac{K\lambda}{\beta \cos\theta}, \tag{1}$$

where $\lambda = 0.1542$ nm is the Cu-Kα wavelength, K is a constant, and β is the FWHM.

3.2 FTIR analysis

FTIR spectroscopy is a significant analytical technique utilized for the qualitative determination of characteristic functional groups, which enable adsorption phenomena. The FTIR spectrum of the prepared PS-NPs is depicted in Figure 2. The FTIR peaks observed, as presented in Table 2, are situated at 461 cm^{-1}, which correspond to the bending of Si–O in Si-(O_4). The peak at 785 cm^{-1} can be attributed to the symmetric stretching vibrations of Si–O–Si. The band observed between 1,000 and 1,300 cm^{-1} corresponds to the stretching modes of the Si–O–Si bonds in PS-NPs.

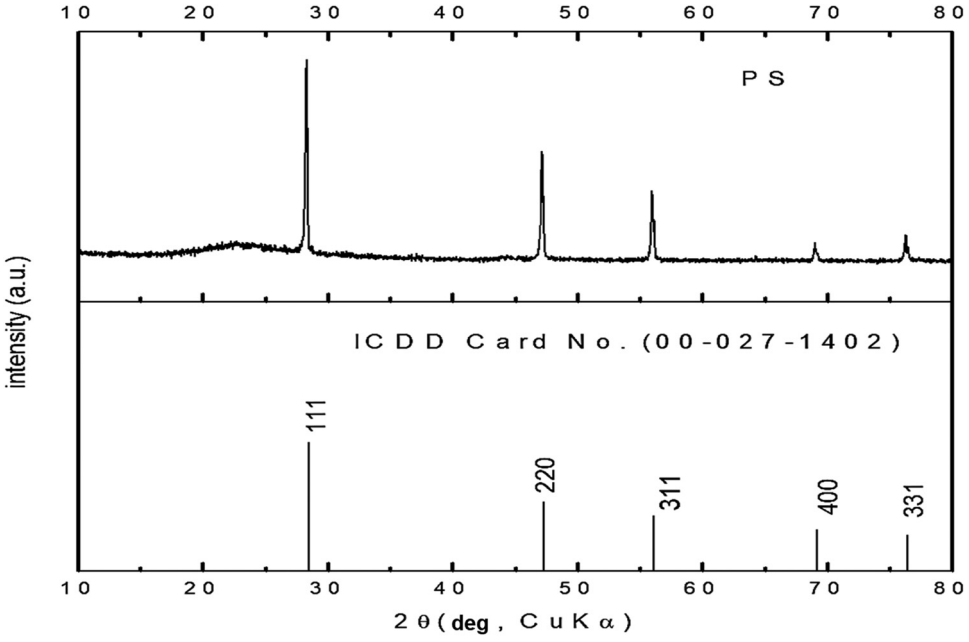

Figure 1: XRD pattern of the prepared PS-NP powder.

Table 1: Crystal sizes of the obtained PS-NPs

Peak	2θ (°)	Plane	FWHM	Size (nm)
1	28.26	(111)	0.2028	42.17
2	47.16	(220)	0.247	36.67
3	55.96	(311)	0.183	51.37
4	69	(400)	0.38	26.51
5	76.28	(331)	0.2017	52.33

The broad band ranging from 3,050 to 3,750 cm^{-1} is associated with the stretching modes of O–H bonds, specifically in the SiOH groups and H_2O molecules. Additionally, the band observed at 1616.4 cm^{-1} can be attributed to the scissor-bending vibration of O–H bonds in water [38].

3.3 Raman spectra analysis

Figure 3 shows the Raman peak of PS-NPs observed at 514 cm^{-1} with a shape that is nearly Lorentzian [40]. The phonons in small crystallites exhibit localization. In the context of crystalline PS, the optical phonon is detected at the central point of the Brillouin zone, exhibiting an energy value of 514 cm^{-1}. This observation can potentially be attributed to the preservation of quasi-momentum within silicon crystals. The crystallinity of the PS-NP powder product agrees with the XRD results as shown in the previous studies [9,41,42]. In a study conducted by Dubey and Gautam [43], it was observed that in the case of pure single-crystalline silicon, the Raman peak occurs at a wavenumber of 520.5 cm^{-1} and exhibits a shape that closely resembles a Lorentzian distribution.

Table 2: FTIR peaks of the prepared PS-NPs

Peak (1/cm)	Functional group/band	Ref
461	Si–O bending	[26]
785	Si–O–Si symmetric stretching vibrations	[39]
1,074	Si–O asymmetric stretching in Si–O–Si	[26]
1616.4	O–H scissor bending vibration	[26]
3,414	O–H stretching modes, interstitial water, and the hydroxyl group	[39]

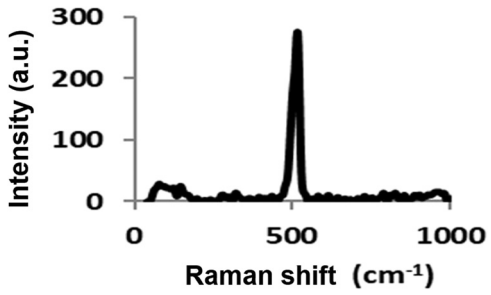

Figure 3: Raman spectra of the PS-NP powder.

3.4 UV-VIS absorbance spectrum analysis

The UV-VIS absorbance spectrum, shown in Figure 4, exhibits the resultant optical properties of the prepared PS-NPs.

The band gap (E_g) of the prepared PS-NPs was estimated by the Tauc plot as well as by a derivative [44]:

$$(\alpha h\upsilon) = A(h\upsilon - E_g)^n. \quad (2)$$

In the given equation, A represents a constant that varies depending on the specific transition; α denotes the

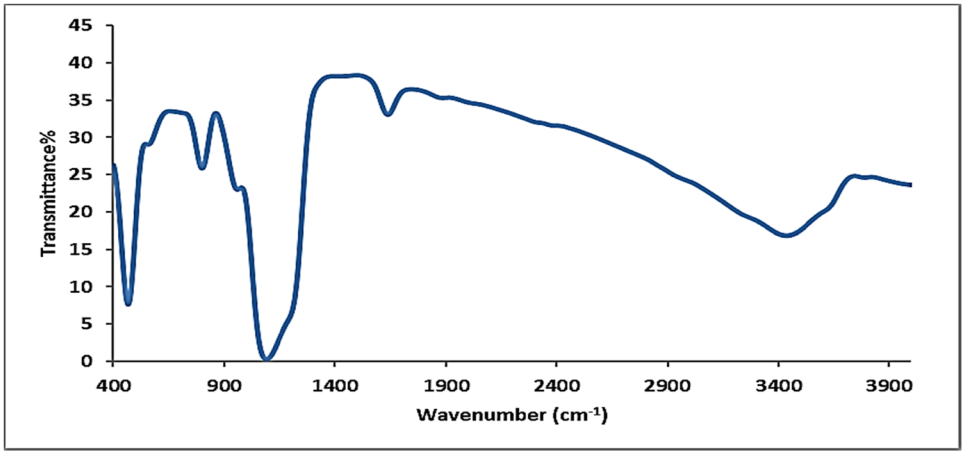

Figure 2: FTIR spectrum of the prepared PS-NP powder.

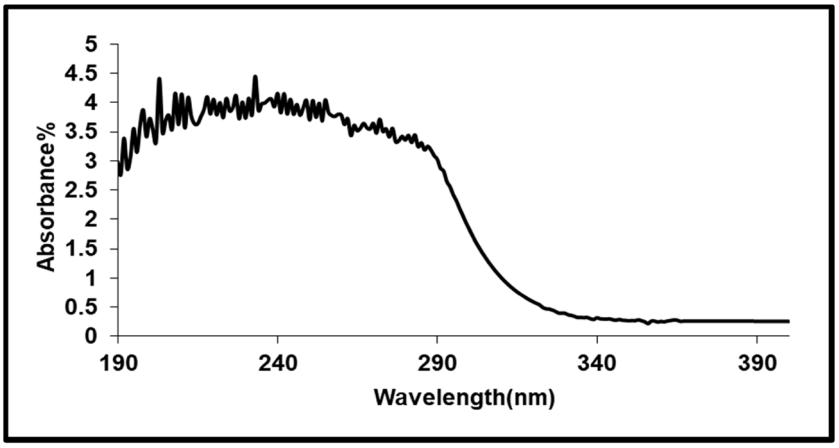

Figure 4: The UV-VIS absorbance spectrum of the PS-NP powder.

absorbance; E_g represents the band gap energy; ($h\nu$) represents the photon energy, with h representing Planck's constant; and n represents an index. The variable n assumes the values of 1/2, 3/2, 2, and 3. The determination of the n value is contingent upon the specific characteristics of the electronic transition that gives rise to the phenomenon of reflection. Figure 5 illustrates the construction of the Tauc plot, where the x-axis represents the photon energy ($h\nu$) and the y-axis represents the square root of the product of photon energy and absorption coefficient ($(h\nu\alpha)^{1/2}$). The band gap energy of the studied material can be determined by extrapolating the linear region to $(h\nu\alpha)^2 = 0$.

3.5 Tauc plot analysis

Figure 5 represents the band gap of the PS-NP powder. It shows the Tauc plot of the prepared PS-NP and its band gap for the indirectly allowed transitions, which equals 3.85 eV. This high band gap value is due to the disturbance of electrons caused by incoming light, and the transition between electronic states is the source of the optical property of a material. Ramadan and Martín-Palma [45] explained that PS-NP particles could be described as a mixture of silicon nanocrystals, amorphous silicon, and air. Therefore, its optical behavior depends on the porosity and thickness

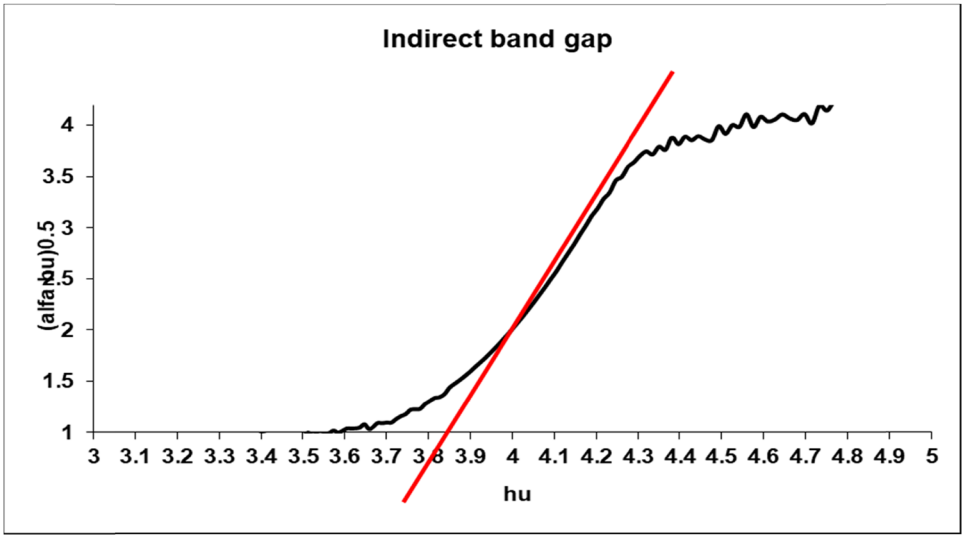

Figure 5: A Tauc plot of the indirect allowed transitions for the prepared PS-NP powder.

of the porous layer. The determined band gap value exhibits a greater magnitude compared to the value reported in a previous study [46].

The phenomenon of bright luminescence in the visible region at room temperature was observed in PS [47]. The visible light emission of PS-NPs can be attributed to various factors, including the direct radiative recombination of confined carriers in Si QDs. (ii) The presence of surface states on the crystallites, which have been contaminated with hydrogen (H) and oxygen (O) due to the chemical etching process, is observed. (iii) The emission of visible light under excitation is attributed to the presence of siloxane. The presence of oxygen-related defect centers has been documented [48]. The emission spectrum is contingent on the specific conditions of the preparation.

3.6 Photoluminescence analysis

Figure 6 shows the photoluminescence of the PS-NP powder. This sample presented a photoluminescence peak at 703 nm. Dubey and Gautam [40] and Salman et al. [49] reported that the photoluminescence peak shifts to a higher wavelength by increasing the porosity and surface area. Then, by increasing the porosity, the value of the energy band gap is increased, and so, the PL peak has a remarkable blue shift.

The average pore diameter (d) for the prepared PS-NPs can be calculated using the following equation [49]:

$$E_g(\text{eV}) = E_g + \frac{h^2}{8d^2}\left|\frac{1}{m_e} + \frac{1}{m_h}\right|, \quad (3)$$

Table 3: Pore size and energy band gap of PS-NPs

Sample	PL peak (nm)	E_g (eV)	Pore size (nm)	Reference
PS-NPs	703	3.85	3.195	This study
PS-wafer	623	2	5.88	[50]
PS-wafer	639	1.940	5.7	[49]
PS-wafer	670	1.85	3.3	[51]

where E (eV) is the energy band gap of PS-NPs, calculated from Figure 6 (experimental value of the PS-NPs PL peak), E_g is the energy band gap of bulk c-Si, h is Planck's constant = 4.13 × 10^{-15} eV s, whereas the electron and hole effective masses are (at 300 K) 0.19m_o, 0.16m_o, and m_o = 9.109 × 10^{-31} kg, respectively. Therefore, the calculated pore size is 3.195 nm. The calculated value of E_g is 3.85 eV, which strongly agrees with the produced value in Figure 5. Table 3 provides a comparison between the values of the synthesized PS-NP powder (pore size and energy band gap) and other published values by different research groups.

3.7 Fungal isolation and morphological identification

The isolation trails from tomato plant parts revealed three fungal isolates that were subjected to morphological examination, and they appeared to be *R. solani*, *Fusarium* sp., and *Botrytis* sp.

R. solani typically appears as a white to brownish, fluffy mycelial growth on the surface of the culture medium. It also produced sclerotia, which were compact, irregularly

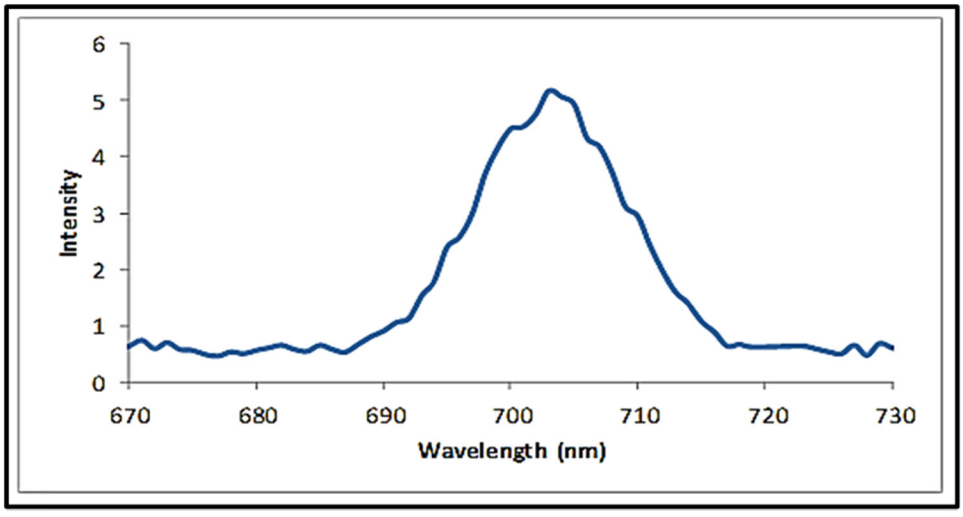

Figure 6: Photoluminescence of the synthesized PS-NP powder.

shaped structures. Under the microscope, *R. solani* showed septate hyphae that lacked cross-walls (non-septate) in some parts. It produced branching, swollen hyphal cells called "beaked" or "barrel-shaped" cells. The presence of clamp connections was a characteristic feature [52].

The isolation of *R. solani* from tomato plants is consistent with previous studies, as this fungal pathogen is known to cause diseases in various crops, including tomatoes [53]. The macroscopic and microscopic features described, such as the production of sclerotia and the presence of clamp connections, align with the characteristics reported in the literature [53,54].

The features in *Fusarium* sp. colonies exhibited a violet color, and textures were fluffy. Meanwhile, the microscopic examination revealed hyaline (colorless) and septate hyphae. The conidiophores bore single or branched chains of conidia. The conidia were usually sickle- or banana-shaped, often with a single-celled or multi-celled macroconidium and sometimes with smaller microconidia [55].

Fusarium sp. is another common fungal pathogen capable of infecting tomato plants and causing various diseases such as *Fusarium* wilt and crown rot [56]. The description of the macroscopic and microscopic features, including the colony color and the presence of sickle-shaped conidia, is consistent with the morphological characteristics of *Fusarium* species [57].

In the Petri-dish, *B. cinerea* colonies initially appeared as a fluffy, whitish-gray mold, which later turned brown or grayish-brown as they produced abundant conidia. The colonies could also exhibit a fuzzy or cottony texture [58]. Under the microscope, *B. cinerea* showed septate hyphae, the conidiophores were typically branched and bore chains of conidia. The conidia were usually colorless or slightly pigmented, ellipsoidal to cylindrical, and had a characteristic "fuzzy" appearance due to the presence of fine hairs or spines. In a previous study, the fungus *B. cinerea* was identified as a necrotrophic pathogen known to infect tomato plants and cause gray mold disease [59]. Also, the description of the macroscopic and microscopic features, such as the production of conidia and the presence of fine hairs or spines on conidia, is in line with previous studies on the morphology of *B. cinerea* [59,60].

Overall, morphological characterization led to the identification of the fungal isolates at the genus level, and for the precise and accurate identification results we investigated at the molecular level. The decision to proceed with molecular identification methods is well-founded, as molecular techniques, such as DNA sequencing and PCR-based methods, can provide more accurate and specific identification of fungal species compared to morphological methods alone [61,62].

3.8 Molecular analysis

Molecular identification results for the fungi isolated from tomato are typically determined through molecular techniques such as PCR and DNA sequencing. These techniques allow for the specific identification and differentiation of fungal species based on their genetic material [55,63]. Also, as reported before, the use of molecular techniques, such as PCR and DNA sequencing, has become standard practice in the identification of fungal species, as these methods offer higher resolution and specificity compared to traditional morphological methods [28,64]. Since the ITS region is widely used for fungal identification due to its highly conserved nature among fungi, making it a suitable target for PCR amplification and DNA sequencing, we used this tool to ensure our isolate identification [65,66]. PCR amplification of the ITS region of the fungal DNA was performed and DNA sequencing of the amplified ITS region revealed a 100% match with *R. solani*, *F. oxysporum*, and *B. cinerea* reference sequences in the GenBank database. Based on these results, the isolated fungi from the tomato samples were identified as *R. solani*, *F. oxysporum*, and *B. cinerea.* The accession numbers were assigned to the sequences OR116524, OR116504, and OR116485, respectively.

The successful identification of *R. solani*, *F. oxysporum*, and *B. cinerea* from tomato plant parts through molecular techniques underscores the importance of combining both morphological and molecular methods in the accurate diagnosis and characterization of plant pathogens.

3.9 Antimicrobial properties

Table 4 displays the growth inhibition percentages of *R. solani*, *F. oxysporum*, and *B. cinerea* when exposed to different concentrations of PS-NPs (μg/mL). The growth inhibition percentages of the fungal pathogens were determined after treating them with various concentrations of PS-NPs. The results indicate that the effectiveness of PS-NPs in inhibiting the growth of these pathogens varied based on the concentration used. At a concentration of 25 μg/mL, PS-NPs exhibited a growth inhibition percentage of 80.00% for *R. solani*, 70.37% for *F. oxysporum*, and 41.11% for *B. cinerea*. Increasing the concentration to 50 μg/mL resulted in slightly lower growth inhibition percentages for all three pathogens: 78.89% for *R. solani*, 71.11% for *F. oxysporum*, and 42.22% for *B. cinerea*.

At a concentration of 75 μg/mL, the growth inhibition percentages showed an improvement compared to the previous concentration. *R. solani* exhibited the highest

Table 4: Growth inhibition percentage of PS-NPs (µg/mL) against *R. solani*, *F. oxysporum*, and *B. cinerea* fungal isolates

Concentration of PS-NPs (µg/mL)	Growth inhibition percentage		
	R. solani	*F. oxysporum*	*B. cinerea*
25	80.00 ab	70.37 c	41.11 d
50	78.89 ab	71.11 bc	42.22 d
75	82.96 a	72.96 ab	44.44 c
100	78.52 b	73.33 a	50 a
Positive control (10 µg/mL)	81.11 ab	71.48 abc	47.78 b
Negative control	0.0 c	0.0 d	0.0 e

Letters a–e in the same column are not the same, and it can be inferred that all the values beside them exhibit statistically significant differences at a probability level of 0.005.

inhibition percentage of 82.96%, followed by *F. oxysporum* at 72.96% and *B. cinerea* at 44.44%. The highest concentration tested, 100 µg/mL, resulted in a slight decrease in growth inhibition percentages compared to 75 µg/mL. *R. solani* showed a percentage of 78.52%, *F. oxysporum* exhibited 73.33%, and *B. cinerea* had the highest inhibition percentage of 50%. Comparing all the concentrations, the positive control with an inhibition percentage of 81.11% for *R. solani*, 71.48% for *F. oxysporum*, and 47.78% for *B. cinerea* showed comparable effectiveness to the highest concentration of PS-NPs. However, the negative control had no inhibitory effect on any of the pathogens. Several results from different studies and investigators proved the ability of metal nanoparticles to exhibit antifungal or antibacterial activity, such as silver nanoparticles, which have been widely investigated for their antifungal properties [1,2,67–69]. The distinctive properties and structural features of PS-NPs, such as their high surface area, unique architecture, and consistent pore dimensions, contribute to their strong antifungal effectiveness against fungal pathogens.

Understanding the mode of action of control agents is essential for enhancing their efficacy, especially when addressing limitations in their performance. The precise mechanism through which PS-NPs combat the studied pathogen remains unclear but several theories have been proposed. The fungicidal activity of PS-NPs may be a result of protein molecule inactivation or direct interaction with the pathogen's DNA, causing DNA mutations and affecting replication [70,71]. The antifungal properties of PS-NPs could be due to the easy degradation of the cell wall resulting from their small size. This degradation occurs by forming hydrogen bonds between the cell wall lipopolysaccharides and the surface hydroxyl groups present in PS-NPs [72]. PS-NP accumulation in the membrane may trigger cell lysis [73] by inhibiting the transmembrane energy cycle, forming insoluble compounds within the fungal membrane that disrupt the electron transport chain, or oxidizing the cell membrane due to the electrostatic attraction between the positively charged PS-NPs and the negatively charged cell membrane [74]. The surface features of PS-NPs support this perspective, as the positively charged PS-NPs interact with protein thiol groups (-SH) on the fungal cell surface, causing cell lysis [75].

The results suggest that the growth inhibition percentages of the fungal pathogens were influenced by the concentration of PS-NPs, with higher concentrations generally exhibiting stronger inhibitory effects. These findings indicate the potential of PS-NPs as a means to control the growth of *R. solani*, *F. oxysporum*, and *B. cinerea*, although further studies are needed to explore their mechanisms of action and evaluate their safety and environmental impact. The antimicrobial activities of PS-NPs were subjectively determined by their characteristics, such as size, shape, concentration, and physicochemical properties [76]. The current results confirmed that the obtained PS-NPs have remarkable antimicrobial capabilities. These studies highlight the potential of various nanoparticles as antifungal agents. However, it is important to consider the potential cytotoxicity, environmental impact, and long-term effects of using nanoparticles before employing them as antifungal agents. Further research should be conducted to optimize the use of nanoparticles and investigate potential synergistic or additive effects with other antifungal agents to enhance their efficacy.

4 Conclusions

In summary, this study has delved into the intriguing realm of utilizing PS-NPs as an environmentally friendly antifungal agent for the management of plant diseases. Our primary objective was to evaluate the efficacy of PS-NPs, synthesized via a free-cell approach, in combating fungal pathogens, aiming to reduce our dependence on synthetic pesticides. This innovative approach holds significant promise for sustainable and eco-friendly plant disease management strategies.

Our investigation has yielded several notable outcomes:

1. **Efficacy of PS-NPs**: Our experiments unveiled a compelling dose-dependent inhibition of fungal growth, spanning a concentration range of 25–100 µg/mL. Impressively, the concentration of 75 µg/mL PS-NPs exhibited the highest growth inhibition percentages compared to the control. This antifungal activity was particularly pronounced against prominent pathogens, including *R. solani*, *F. oxysporum*, and *B. cinerea*.

2. **Structural characterization**: Employing various characterization techniques, such as X-ray powder diffraction, FTIR spectroscopy, Raman spectroscopy, UV-VIS absorbance, and photoluminescence, we have confirmed the nanocrystalline structure and crystalline quality of PS-NPs. This deeper structural understanding enriches our grasp of their antimicrobial potential.
3. **Environmental sustainability**: The utilization of ultrasonication for PS-NP synthesis has emerged as a safe, cost-effective, and environmentally friendly methodology. This aspect underscores the potential for eco-conscious alternatives in the realm of plant disease management.
4. **Novelty and implications**: This study marks a pioneering exploration of PS-NPs as antifungal agents, representing the first *in vitro* evaluation of their efficacy. The amalgamation of their unique structural characteristics and potent antifungal properties suggests wide-ranging applications in various technological sectors.

Our research underscores the immense promise of PS-NPs in the context of sustainable plant disease management. It underscores their dual advantages of environmental friendliness and effectiveness in inhibiting fungal pathogens. Furthermore, our work not only contributes to the existing body of knowledge regarding alternative disease management strategies but also kindles the spark for future research and practical applications.

Our vision for future work envisions an extended exploration of PS-NPs in diverse agricultural and industrial settings. We anticipate conducting comparative studies to establish quantitative benchmarks, providing a clear metric for their performance relative to established treatments. This continued research trajectory will serve as a crucial step in advancing sustainable and efficacious approaches to plant disease control, ultimately benefitting both agriculture and the environment.

Acknowledgements: The authors express their sincere thanks to the City of Scientific Research and Technological Applications (SRTA-City) and the Faculty of Agriculture (Saba Basha), Alexandria University, Egypt, for providing the necessary research facilities. The authors would like to extend their appreciation to the Researchers Supporting Project (number RSP2024R505), King Saud University, Riyadh, Saudi Arabia.

Funding information: This research was financially supported by the Researchers Supporting Project (number RSP2024R505), King Saud University, Riyadh, Saudi Arabia.

Author contributions: Methodology and writing – original manuscript; M.N., M.E., A.A.Al., P.K., A.A., and S.I.B., project validation; A.A. and A.A.Al., investigation; M.N., M.E., A.A., and S.I.B., reviewing; M.N., M.E., P.K., A.A., and S.I.B. All the authors agreed on the final version of the manuscript.

Conflict of interest: The authors declare no conflict of interest.

Ethical approval: The conducted research is not related to either human or animal use.

Data availability statement: The data used to support the findings of this study are available from the corresponding author upon request.

References

[1] Kamel SM, Elgobashy SF, Omara RI, Derbalah AS, Abdelfatah M, El-Shaer A, et al. Antifungal activity of copper oxide nanoparticles against root rot disease in cucumber. J Fungi. 2022;8:911.
[2] Elkobrosy D, Al-Askar AA, El-Gendi H, Su Y, Nabil R, Abdelkhalek A, et al. Nematocidal and bactericidal activities of green synthesized silver nanoparticles mediated by ficus sycomorus leaf extract. Life. 2023;13:1083.
[3] Hazarika A, Yadav M, Yadav DK, Yadav HS. An overview of the role of nanoparticles in sustainable agriculture. Biocatal Agric Biotechnol. 2022;43:102399. doi: 10.1016/j.bcab.2022.102399.
[4] Bao-Shan L, shao-qi D, Chun-Hui L, Li-Jun F, Shu-Chun Q, Min Y. Effect of TMS (nanostructured silicon dioxide) on growth of Changbai larch seedlings. J For Res. 2004;15:138–40.
[5] Mogoda AS, Farag AR. The effects of a few formation parameters on porous silicon production in HF/HNO3 using ag-assisted etching and a comparison with a stain etching method. Silicon. 2022;14:11405–15.
[6] Kashyout A-H, Nabil M. Production of high throughput nano-porous silicon (NPS) powder with different architectures. Mater Chem Phys. 2018;216:454–9.
[7] Hadi HA, Ismail RA. Preparation and Characteristics Study of High-Quantum Efficiency Ni/PSi/c-Si and cd/PSi/c-Si Double-Junction Photodetectors. Silicon. 2022;14:11089–96.
[8] Muduli RC, Kale P. Synergetic effect of porous silicon–Nickel composite on its solid-state hydrogen energy storage properties. Int J Hydrog Energy. 2023;48:35185–96.
[9] Nabil MM, Mahmoud KM, Nomeir R, El-Maghraby E-M, Motaweh H. 3D porous silicon (nanorods array, nanosheets, and nanoclusters) production. Egypt J Chem. 2020;63:1269–78.
[10] Kalantari F, Amirmazlaghani M, Olyaee S. Enhanced UV-sensing properties by utilizing solution-processed GQD in GQDs/Porous Si heterojunction Near-UV photodetector. Mater Sci Semicond Process. 2023;163:107560.
[11] Koyuda DA, Titova SS, Tsurikova UA, Kakuliia IS, Parinova EV, Chuvenkova OA, et al. Composition and electronic structure of porous silicon nanoparticles after oxidation under air-or freeze-drying conditions. Mater Lett. 2022;312:131608.
[12] Elyamny S, Eltarahony M, Abu-Serie M, Nabil MM. Kashyout AE-HB. One-pot fabrication of Ag@ Ag2O core–shell nanostructures for biosafe antimicrobial and antibiofilm applications. Sci Rep. 2021;11:22543.

[13] Azimi R, Borzelabad MJ, Feizi H, Azimi A. Interaction of SiO nanoparticles with seed prechilling on germination and early seedling growth of tall wheatgrass (Agropyron elongatum L.). Polish J Chem Technol. 2014;16:25–9.
[14] Wang L, Ning C, Pan T, Cai K. Role of silica nanoparticles in abiotic and biotic stress tolerance in plants: A review. Int J Mol Sci. 2022;23:1947. doi: 10.3390/ijms23041947.
[15] Nair R, Varghese SH, Nair BG, Maekawa T, Yoshida Y, Kumar DS. Nanoparticulate material delivery to plants. Plant Sci. 2010;179:154–63.
[16] Siddiqui MH, Al-Whaibi MH, Faisal M, Al Sahli AA. Nano-silicon dioxide mitigates the adverse effects of salt stress on Cucurbita pepo L. Environ Toxicol Chem. 2014;33:2429–37.
[17] Haghighi M, Afifipour Z, Mozafarian M. The effect of N-Si on tomato seed germination under salinity levels. J Biol Environ Sci. 2012;6:87–90.
[18] Suriyaprabha R, Karunakaran G, Kavitha K, Yuvakkumar R, Rajendran V, Kannan N. Application of silica nanoparticles in maize to enhance fungal resistance. IET Nanobiotechnol. 2014;8:133–7.
[19] Hasan KA, Soliman H, Baka Z, Shabana YM. Efficacy of nano-silicon in the control of chocolate spot disease of Vicia faba L. caused by Botrytis fabae. Egypt J Basic Appl Sci. 2020;7:53–66.
[20] Derbalah A, Shenashen M, Hamza A, Mohamed A, El Safty S. Antifungal activity of fabricated mesoporous silica nanoparticles against early blight of tomato. Egypt J Basic Appl Sci. 2018;5:145–50.
[21] Khan MR, Siddiqui ZA. Use of silicon dioxide nanoparticles for the management of Meloidogyne incognita, Pectobacterium betavasculorum and Rhizoctonia solani disease complex of beetroot (Beta vulgaris L.). Sci Hortic (Amsterdam). 2020;265:109211.
[22] Elamawi RM, Tahoon AM, Elsharnoby DE, El-Shafey RA. Bio-production of silica nanoparticles from rice husk and their impact on rice bakanae disease and grain yield. Arch Phytopathol Plant Prot. 2020;53:459–78.
[23] El-Shetehy M, Moradi A, Maceroni M, Reinhardt D, Petri-Fink A, Rothen-Rutishauser B, et al. Silica nanoparticles enhance disease resistance in Arabidopsis plants. Nat Nanotechnol. 2021;16:344–53.
[24] Behiry S, Soliman SA, Massoud MA, Abdelbary M, Kordy AM, Abdelkhalek A, et al. Trichoderma pubescens Elicit Induced Systemic Resistance in Tomato Challenged by Rhizoctonia solani. J Fungi. 2023;9:167. doi: 10.3390/jof9020167.
[25] Abd El-Rahim WM, Mostafa EM, Moawad H. High cell density cultivation of six fungal strains efficient in azo dye bioremediation. Biotechnol Rep. 2016;12:1–5.
[26] Nabil M, Mahmoud KR, Nomier R, El-Maghraby E-M, Motaweh H. Nano-Porous-Silicon Powder as an Environmental Friend. Materials (Basel). 2021;14:4252.
[27] Soliman SA, Al-Askar AA, Sobhy S, Samy MA, Hamdy E, Sharaf OA, et al. Differences in Pathogenesis-Related Protein Expression and Polyphenolic Compound Accumulation Reveal Insights into Tomato–Pythium aphanidermatum Interaction. Sustainability. 2023;15:6551.
[28] White TJ, Bruns T, Lee S, Taylor J. Amplification and direct sequencing of fungal ribosomal RNA genes for phylogenetics. PCR Protocols: a Guide to Methods and Applications. New York: Academic Press, Inc.; Vol. 18; 1990. p. 315–22.
[29] Kumar A, Shukla R, Singh P, Prasad CS, Dubey NK. Assessment of Thymus vulgaris L. essential oil as a safe botanical preservative against post harvest fungal infestation of food commodities. Innov Food Sci Emerg Technol. 2008;9:575–80.
[30] Khamis WM, Heflish AA, El-Messeiry S, Behiry SI, Al-Askar AA, Su Y, et al. Swietenia mahagoni Leaves Extract: Antifungal, Insecticidal, and Phytochemical Analysis. Separations. 2023;10:301.
[31] Al-Askar AA, Bashir S, Mohamed AE, Sharaf OA, Nabil R, Su Y, et al. Antimicrobial Efficacy and HPLC Analysis of Polyphenolic Compounds in a Whole-Plant Extract of Eryngium campestre. Separations. 2023;10:362.
[32] Nabil M. Photoluminescence emission control of porous silicon. Soft Nanosci Lett. 2019;9:35–44.
[33] Nabil MM, Motaweh H. Synthesis, antimicrobial, antioxidant and docking study of studying the wetting agent impact in the porous silicon production. Egypt J Chem. 2020;63:1849–55.
[34] Nabil M, Mahmoud KR, El-Shaer A, Nayber HA. Preparation of crystalline silica (quartz, cristobalite, and tridymite) and amorphous silica powder (one step). J Phys Chem Solids. 2018;121:22–6.
[35] Nabil M, Motaweh HA. Shape control of silica powder formation. J Mater Sci Chem Eng. 2019;7:49–55.
[36] Fakhri MA, Alwahib AA, Salim ET, Ismail RA, Amir HAAA, Ibrahim RK, et al. Preparation and characterization of UV-enhanced GaN/porous Si photodetector using PLA in liquid. Silicon. 2023;15:7523–40.
[37] Ramadan M, Elnouby MS, El-Shazly O, El-Wahidy EF, Farag AAM, Roushdy N. Facile fabrication, structural and electrical investigations of cadmium sulfide nanoparticles for fuel cell performance. Mater Renew Sustain Energy. 2022;11:277–86.
[38] Khalifa M, Hajji M, Ezzaouia H. Purification of silicon powder by the formation of thin porous layer followed byphoto-thermal annealing. Nanoscale Res Lett. 2012;7:1–4.
[39] Nabil M, Elnouby M, Gayeh N, Sakr AH, Motaweh HA. Enhancement of porous silicon photoluminescence using (Ni) treatment. IOP Conf Ser Mater Sci Eng. 2017;248:12001. IOP Publishing.
[40] Dubey RS, Gautam DK. Fabrication and characterization of porous silicon layers for applications in optoelectronics. Opt Quantum Electron. 2009;41:189–201.
[41] Melinon P, Keghelian P, Prével B, Dupuis V, Perez A, Champagnon B, et al. Structural, vibrational, and optical properties of silicon cluster assembled films. J Chem Phys. 1998;108:4607–13.
[42] Spallino L, Vaccaro L, Sciortino L, Agnello S, Buscarino G, Cannas M, et al. Visible-ultraviolet vibronic emission of silica nanoparticles. Phys Chem Chem Phys. 2014;16:22028–34.
[43] Dubey RS, Gautam DK. Synthesis and characterization of nanocrystalline porous silicon layer for solar cells applications. J Optoelectron Biomed Mater. 2009;1:8–14.
[44] Ashery MH, Elnouby M, EL-Maghraby EM, Elsehly EM. Structural control of V2O5 nanoparticles via a thermal decomposition method for prospective photocatalytic applications. Beni-Suef Univ J Basic Appl Sci. 2023;12:1–15.
[45] Ramadan R, Martín-Palma RJ. The Infiltration of Silver Nanoparticles into Porous Silicon for Improving the Performance of Photonic Devices. Nanomaterials. 2022;12:271.
[46] Khudiar SS, Nayef UM, Mutlak FA-H, Abdulridha SK. Characterization of NO2 gas sensing for ZnO nanostructure grown hydrothermally on porous silicon. Optik (Stuttg). 2022;249:168300.
[47] Koshida N, Canham LT. Thermal properties of porous silicon. Handbook of Porous Silicon. 2nd edn. New York: Springer; 2017. p. 309–18.
[48] Kumar S, Dixit PN, Rauthan CMS, Parashar A, Gope J. Effect of power on the growth of nanocrystalline silicon films. J Phys Condens Matter. 2008;20:335215.

[49] Salman KA, Hassan Z, Omar K. Effect of silicon porosity on solar cell efficiency. Int J Electrochem Sci. 2012;7:376–86.
[50] Chan KS, Dwight TJE. Photoluminescence, morphological and electrical properties of porous silicon formulated with different HNO3 concentrations. Result Phys. 2018;10:5–9.
[51] Alwan AM, Naseef IAN. Optimization of photoluminescence properties of Porous silicon by adding gold nanoparticles. Iraqi J Sci. 2017;58(1A):53–62.
[52] Heflish AA, Behiry SI, Al-Askar AA, Su Y, Abdelkhalek A, Gaber MK. Rhaphiolepis indica Fruit Extracts for Control Fusarium solani and Rhizoctonia solani, the Causal Agents of Bean Root Rot. Separations. 2023;10:369.
[53] Sneh B, Burpee L, Qgoshi A. Identification of Rhizocto- nia species. USA: APS Press; 1991.
[54] Ogoshi A. Introduction – the genus Rhizoctonia. In: Sneh B, Jabaji-Hare S, Neate S, Dijst G, editors. Rhizoctonia species: Taxonomy, molecular biology, ecology, pathology and disease control. Dordrecht: Springer; 1996. p. 1–9.
[55] Sobhy S, Al-Askar AA, Bakhiet EK, Elsharkawy MM, Arishi AA, Behiry SI, et al. Phytochemical characterization and antifungal efficacy of camphor (Cinnamomum camphora L.) extract against phytopathogenic fungi. Separations. 2023;10:189.
[56] Agrios GN. Plant Pathology. 5th Edition. Amsterdam: Elsevier Academic Press; 2005. doi: 10.1016/C2009-0-02037-6.
[57] Leslie JF, Summerell BA. The Fusarium Laboratory Manual. Ames, Iowa, USA: Blackwell Publishing; 2007. doi: 10.1002/9780470278376.
[58] El-Bilawy EH, Al-Mansori A-NA, Soliman SA, Alotibi FO, Al-Askar AA, Arishi AA, et al. Antifungal, antiviral, and HPLC analysis of phenolic and flavonoid compounds of amphiroa anceps extract. Sustainability. 2022;14:12253.
[59] Elad Y, Williamson B, Tudzynski P, Delen N. Botrytis spp. and diseases they cause in agricultural systems–an introduction. In: Elad Y, Williamson B, Tudzynski P, Delen N, editors. Botrytis: Biology, Pathology and Control. Dordrecht: Springer; 2007. p. 1–8.
[60] Williamson B, Tudzynski B, Tudzynski P, Van Kan JAL. Botrytis cinerea: the cause of grey mould disease. Mol Plant Pathol. 2007;8:561–80.
[61] Carbone I, Kohn LM. A method for designing primer sets for speciation studies in filamentous ascomycetes. Mycologia. 1999;91:553–6.
[62] O'Donnell K, Cigelnik E. Two divergent intragenomic rDNA ITS2 types within a monophyletic lineage of the fungusfusariumare nonorthologous. Mol Phylogenet Evol. 1997;7:103–16.
[63] Bellemain E, Carlsen T, Brochmann C, Coissac E, Taberlet P, Kauserud H. ITS as an environmental DNA barcode for fungi: an in silico approach reveals potential PCR biases. BMC Microbiol. 2010;10:1–9.
[64] Abdelkhalek A, Al-Askar AA, Arishi AA, Behiry SI. Trichoderma hamatum strain Th23 promotes tomato growth and induces systemic resistance against tobacco mosaic virus. J Fungi. 2022;8:228.
[65] Schocha CL, Seifertb KA, Huhndorfc S, Robertd V, Spougea JL, Levesqueb CA, et al. Nuclear ribosomal internal transcribed spacer (ITS) region as a universal DNA barcode marker for Fungi. PNAS. 2012;109:6241–6.
[66] Youssef NH, Qari SH, Behiry SI, Dessoky ES, El-Hallous EI, Elshaer MM, et al. Antimycotoxigenic activity of beetroot extracts against altenaria alternata mycotoxins on potato crop. Appl Sci. 2021;11:4239.
[67] Mosa WFA, Behiry SI, Ali HM, Abdelkhalek A, Sas-Paszt L, Al-Huqail AA, et al. Pomegranate trees quality under drought conditions using potassium silicate, nanosilver, and selenium spray with valorization of peels as fungicide extracts. Sci Rep. 2022;12:6363. doi: 10.1038/s41598-022-10354-1.
[68] Mosa WFA, Mackled MI, Abdelsalam NR, Behiry SI, Al-Askar AA, Basile A, et al. Impact of silver nanoparticles on lemon growth performance: insecticidal and antifungal activities of essential oils from peels and leaves. Front Plant Sci. 2022;13:1–15. doi: 10.3389/fpls.2022.898846.
[69] Hamdy E, Al-Askar AA, El-Gendi H, Khamis WM, Behiry SI, Valentini F, et al. Zinc oxide nanoparticles biosynthesized by eriobotrya japonica leaf extract: characterization, insecticidal and antibacterial properties. Plants. 2023;12:2826.
[70] Petica A, Gavriliu S, Lungu M, Buruntea N, Panzaru C. Colloidal silver solutions with antimicrobial properties. Mater Sci Eng B. 2008;152:22–7.
[71] Salem HF, Eid KAM, Sharaf MA. Formulation and evaluation of silver nanoparticles as antibacterial and antifungal agents with a minimal cytotoxic effect. Int J Drug Deliv. 2011;3:293–304.
[72] Capeletti LB, de Oliveira LF, Goncalves K de A, de Oliveira JFA, Saito A, Kobarg J, et al. Tailored silica–antibiotic nanoparticles: overcoming bacterial resistance with low cytotoxicity. Langmuir. 2014;30:7456–64.
[73] Gill SR, Fouts DE, Archer GL, Mongodin EF, DeBoy RT, Ravel J, et al. Insights on evolution of virulence and resistance from the complete genome analysis of an early methicillin-resistant Staphylococcus aureus strain and a biofilm-producing methicillin-resistant Staphylococcus epidermidis strain. J Bacteriol. 2005;187:2426–38.
[74] Rezaei ZS, Javed A, Ghani MJ, Soufian S, Barzegari FF, Bayandori MAM, et al. Comparative study of antimicrobial activities of TiO_2 and CdO nanoparticles against the pathogenic strain of Escherichia coli. Iran J Pathol. 2010;5:83–9.
[75] Zhang H, Chen G. Potent antibacterial activities of Ag/TiO2 nanocomposite powders synthesized by a one-pot sol− gel method. Environ Sci Technol. 2009;43:2905–10.
[76] El-Moslamy SH, Elnouby MS, Rezk AH, El-Fakharany EM. Scaling-up strategies for controllable biosynthetic ZnO NPs using cell free-extract of endophytic Streptomyces albus: characterization, statistical optimization, and biomedical activities evaluation. Sci Rep. 2023;13:3200.